Three-Dimensional Metallic Photonic Crystals with Optical Bandgaps

*Nikos Vasilantonakis, Konstantina Terzaki, Ioanna Sakellari, Vytautas Purlys, David Gray, Costas M. Soukoulis, Maria Vamvakaki, Maria Kafesaki, and Maria Farsari**

Over the last few years, there has been an increasing interest in nanoscale metallic photonic crystals (PCs), i.e., periodic systems of metal nanostructures. This interest is connected mainly with the potential electromagnetic functionalities of these structures, which are not observed in bulk materials.[1–3] Metallic PCs significantly modify the properties of light with wavelength close to their periodicity, resulting in potential applications in scientific and technical areas such as filters, optical switches, sensing, imaging, energy harvesting and photovoltaics, cavities and efficient laser designs.[4]

Studies of metallic PCs have mostly concentrated on microwave, millimeter wave and far-infrared frequencies.[5–9] At these frequencies, metals act like nearly perfect reflectors and have no significant absorption problems. There is an interest to fabricate 3D metallic PCs at far-infrared and optical frequencies, usually using the woodpile geometry,[10] to produce efficient thermal emitters and photovoltaic devices, through tailoring their absorption spectrum.

The main reason for the current lack of 3D metallic PCs at optical wavelengths is that the fabrication of three-dimensional metallic, high resolution structures is a challenging task. Most of the 3D, submicron-scale metallic PCs that have been obtained so far are based on metal infiltration of self-organized inverse opal structures.[11–13] This kind of structures do not allow fabrication control of long-range monocrystals, due to the self-organization underlying approach. Some effort has been made to directly fabricate metallic 3D structures using multiphoton reduction of metal ions. The quality of the structures, however, has been compromised by the reduced transparency of the metal ion solutions at the laser wavelengths used (500–800 nm).[14,15] Metallic woodpile structures have also been realized experimentally at micron wavelengths using traditional lithographic techniques.[16–18] However, lithographic techniques can accommodate only a very limited number of layers, and aligning each layer with the previous one is not a trivial issue.

To date, the most popular and successful method for the fabrication of 3D metallic nanostructures is the preparation of 3D dielectric templates using Direct fs Laser Writing (DLW), and their subsequent metallization.[19–21] DLW by multiphoton polymerization is a direct laser writing technique that allows the construction of 3D structures with resolution beyond the diffraction limit.[22–24] The polymerization process is due to nonlinear absorption within the focal volume, initiated by a focused ultrafast laser beam. Employing laser intensities that are only slightly above the nonlinear polymerization threshold, structures with very high resolution can be made.[25,26] In classic DLW, the lateral resolution is limited to about 100 nm. This value obviously cannot compete with state-of-the-art electron-beam lithography, where 10 nm are readily accessible. However, recent work using stimulated-emission depletion DLW[27] has approached 50-nm lateral resolution, with potential for future improvements. Moreover, the recent increased interest in optical metamaterials,[28] in connection with imaging applications,[29] has given an additional boost in research on nanosale metallic periodic systems.[4,28]

When a positive photoresist is structured using DLW lithography, the result is a bulk structure with voids in the desired shape. These voids can be filled with gold using electroplating,[30] an extremely simple and inexpensive setup. One merely applies a bias voltage between a transparent electrode on the substrate and a macroscopic counter electrode within a beaker.

When a negative photoresist is structured, the result is a dielectric template. To metalize this template, one can use atomic-layer deposition of silica or titania onto it, followed by chemical vapour deposition of silver.[31] The technique most commonly used for the subsequent metallization of these templates, however, is electroless plating (EP). EP is a fairly simple process that doesn't require any specialized equipment, and the metal deposition can be done without using any electrical potential.[32,33] In general it is characterized by the selective reduction of metal ions at the surface of a catalytic substrate immersed into an aqueous solution of metal ions, with continued deposition on the substrate through the catalytic action of the deposit itself. One approach is to use a standard photolithographic material, such as the negative photoresist SU8 for the fabrication of the structures, and subsequently activate their surface.[34,35] In this case additional processing, to enable the metal adhesion on the surface, is required and the quality, structural integrity and resolution of the structures depends on the building material

N. Vasilantonakis, K. Terzaki, Dr. I. Sakellari, V. Purlys, Dr. D. Gray, Prof. C. M. Soukoulis, Prof. M. Vamvakaki, Prof. M. Kafesaki, Dr. M. Farsari
Institute of Electronic Structure and Laser (IESL)
Foundation for Research and Technology - Hellas (FORTH)
N. Plastira 100, 70013 Heraklion, Greece
E-mail: mfarsari@iesl.forth.gr

N. Vasilantonakis, K. Terzaki, Prof. M. Vamvakaki, Prof. M. Kafesaki
Department of Materials Science and Technology
University of Crete
Heraklion, Crete, Greece

Prof. C. M. Soukoulis
Ames Laboratory and Department of Physics and Astronomy
Iowa State University
Ames, IA 50011, USA

DOI: 10.1002/adma.201104778

and the surface processing step. The resolution and structure integrity can be very good; however, as the density of the metal binding sites on the structure cannot be controlled, the metallization quality can vary. In addition, along with the surface of the structures, the substrate is also activated; the metallization is therefore not selective, often requiring an extra step to remove the structures from the metalized substrate.[35] This is addressed by an alternative approach, which employs a photopolymer doped with the metal binding sites. In this case, the metallization is selective, the density and distribution of the binding sites can be controlled, and the resolution, structural integrity, and metallization quality limitations derive only from the photopolymer used.[36] To date, the DLW approach with subsequent metallization has been applied up to now with great success in the realization of infrared metamaterials.[28,35,37]

Here, we report the nanofabrication of 3D metallic woodpile structures with features below 100 nm, obtained by DLW and selective silver coating. The structures, which have fcc geometry[10] and in-layer periodicity 600 nm, are fabricated using an organic inorganic, zirconium-silicon hybrid material doped with a metal-binding monomer, 2-(dimethylamino) ethyl methacrylate. They are subsequently metalized using electroless plating. The metalized structures are shown to exhibit ohmic conductivity, comparable to pure silver. We also present here experimental and theoretical electromagnetic characterization results of the fabricated structures, showing a cut-off at around 300 THz (1 μm) and a second band gap inside the optical part of the spectrum, centered at 450 THz. To the best of our knowledge this is the first time that metalized structures with such resolution, ohmic response, and band gaps in the visible are fabricated and characterized.

In what follows we discuss firstly the structure fabrication and metallization steps, we continue with the resistance measurements, which demonstrate the ohmic response of the structure, and with the structural characterization, which demonstrates the long range-order characterizing our structures and provides the geometrical features used in the simulations. Finally we discuss the experimental and theoretical electromagnetic characterization of the structures, through transmission measurements and simulations, which reveal a bandgap in the visible range.

The photosensitive material used for the fabrication of the three dimensional photonic nanostructures is a zirconium-silicon organic-inorganic material doped with tertiary amine metal-binding moieties.[38] Hybrid (organic-inorganic) materials are a very popular class of photosensitive materials, as they are easy to prepare, modify and photopolymerize and, after polymerization, they are optically, mechanically and chemically stable. As a result, the have found many applications in 3D photonic and biomedical devices.[39,40] In addition, hybrid materials chemistry provides the possibility of the inclusion of functional groups, such as nonlinear optical molecules and quantum dots.[41,42] Building on our previous work on the synthesis and DLW processing of a silicon-zirconium hybrid material,[43,44] we have added methacrylate moieties by adding a 2-(dimethylamino) ethyl methacrylate (DMAEMA) monomer, capable of participating in the photopolymerization step to incorporate covalently bound metal-binding groups in the 3D structures.[38]

The main materials used here for the synthesis of photopolymer were methacryloxy-propyltrimethoxysilane (MAPTMS, 99%), dimethyl-aminoethyl methacrylate (DMAEMA, >99%) and zirconium *n*-propoxide (ZPO) 70% solution in 1-propanol. The molar ratios were 7:3 for MAPTMS/ZPO and 3:7 for DMAEMA/MAPTMS. MAPTMS was firstly hydrolyzed by adding HCl (0.1 M) at a 1:0.1 ratio and the mixture was stirred for 20 minutes. Next, ZPO was mixed with DMAEMA and the mixture was stirred for 15 min. The MAPTMS sol was gently added to the stirred ZPO sol and the mixture was stirred for 30 min. Finally, the photoinitiator 4,4-bis(diethylamino) benzophenone was added at a 1% w/w concentration to the final solution. The solution was filtered using 0.2 μm syringe filters. Before structuring, a small droplet of the composite solution was placed on a on a 100 micron thick glass slide and heated at 50 °C for 30 min. After DLW processing, the sample was developed and the material not exposed to the laser radiation removed by immersion in a 7:3 isopropanol/1-propanol solution. The metallization procedure has been described in detail previously.[38]

For the 3D structuring a Ti:Sapphire femtosecond laser (800 nm, 75 MHz, <20 fs) was focused into the photopolymerisable composite using a high numerical aperture focusing microscope objective lens (100×, N.A. = 1.4, Zeiss, Plan Apochromat). Sample movement was achieved using piezoelectric and linear stages, for accurate and step movement, respectively (PI). The whole DLW setup, which is described in detail in Ref. [45], was computer-controlled using the 3DPoli software. Here, the average laser power used for the fabrication of the high-resolution structures was 18 mW, measured before the objective, while the average transmission to the sample was 20%. To avoid contact with the lens immersion oil, all structures were fabricated upside down with the glass substrate in contact with the oil. They were built layer-by-layer starting from the top with the last layer adhering to the substrate. This way, the laser beam did not cross an already polymerized layer, causing second polymerization or beam distortion.

In order to measure the conductivity of the metalized structures, solid bulk dielectric boxes were created and metalized via electroless plating, keeping the same conditions as in the woodpile structures, and the resistance at the faces of those boxes was measured. The equipment used for the measurement was a Tektronix 370 curve tracer, which monitors the current, *I*, for each specific voltage, *V*, applied between the two metallic needles of the tracer which are placed on the samples. Modifying the voltage we observed the linear *I*–*V* response of the structures, and thus their Ohmic behavior, with average resistance $R = (3.46 \pm 0.21)\ \Omega$. Calculation of the resistivity, ρ, taking into account the needle size and the thickness of the metal gave $\rho = (1.75 \pm 1.15) \cdot 10^{-7}\ \Omega \cdot m$, and, thus, conductivity $\sigma = 1/\rho = (5.71 \pm 3.01) \cdot 10^{6}\ \Omega^{-1} \cdot m^{-1}$. This result is close to the conductivity of pure silver, which is $6.3 \cdot 10^{7}\ \Omega^{-1} \cdot m^{-1}$ (DC value). The thickness of the metal was estimated from SEM images of structures before and after metallization and was found to be in the range ~30–50 nm.

Figure 1 shows the Scanning Electron Microscope (SEM) pictures of some typical metalized woodpile structures with two different periodicities, showing the flexibility and the high resolution that can be achieved using this fabrication technology. In order to achieve maximum resolution, the lowest intensity that was enough to fabricate fully 3D structures was used.

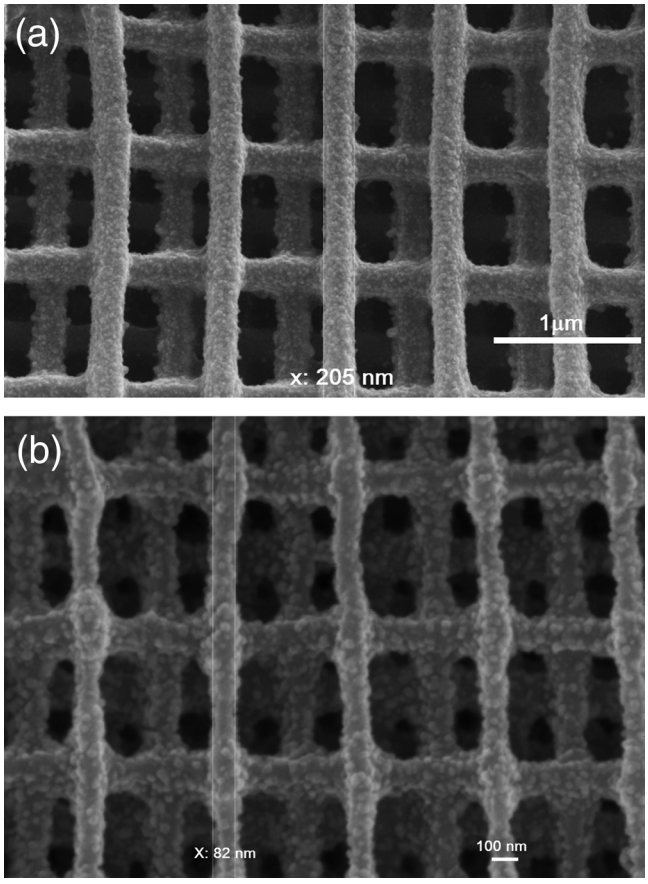

Figure 1. Metalized woodpile structures at 900 nm (a) and 600 nm (b) periodicity. The value at the bottom left corner depicts the average thickness of the rods.

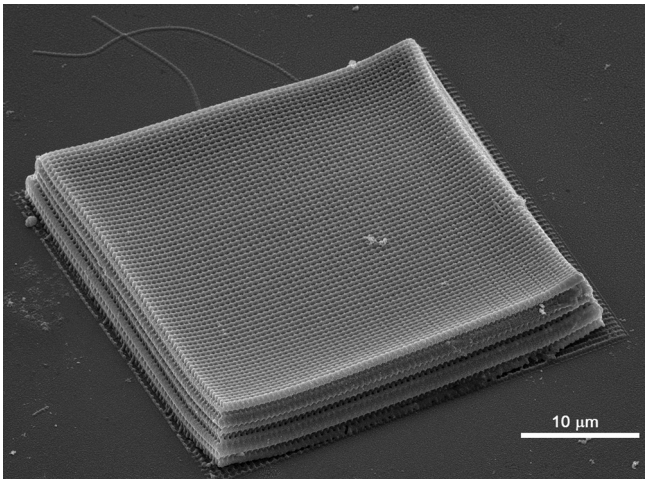

Figure 2. Perspecitive view of a 600 nm periodicity and 3-unit-cell (12-layer) thickness woodpile structure.

Figure 2 shows a metalized woodpile structure with 600 nm periodicity fabricated using 1.90 mW laser power. This structure has 3 unit cells (12 layers) thickness and its features are in the order of 100 nm.

For the transmission measurements a white light source pumped at 1064 nm (Fianium) was used. The light beam was focused normally to the sample surface using a 7.5 cm focal length lens, while the transmitted light was collected using an optical spectrometer (Ocean Optics S2000). The half-opening angle of the incident light was 5°, assured by iris diaphragms. The diameter of the focused beam in the sample was 24 μm, while the measured nanostructure surface normal to the beam was 40 μm × 40 μm. As the size of the sample's surface was comparable to the beam spot diameter, sample alignment was difficult and critical. To check the alignment, but also to check the quality of the sample, the diffraction pattern in the reflected waves produced by the structure when illuminated by the white light beam was used. **Figure 3** shows a typical such diffraction pattern. To understand the diffraction pattern one should note that the woodpile structure presents the {001} family of planes parallel to the crystal surface - the direction normal to these planes is referred as Γ*X*, which is the one studied. In these planes the structure presents a square symmetry, that is actually revealed by the square symmetry of the diffraction pattern observed.[46] The sharpness of the diffraction spots indicates the long-range order in the crystal.

As already described by several groups,[46,47] diffraction channels for normal incidence are open when the incident wave vector **k** is larger in magnitude than any of the 2D reciprocal lattice vectors, **g**, of the planes parallel to the crystal surface. A diffraction cutoff is observed whenever $|\mathbf{g}| = |\mathbf{k}|$. For a square

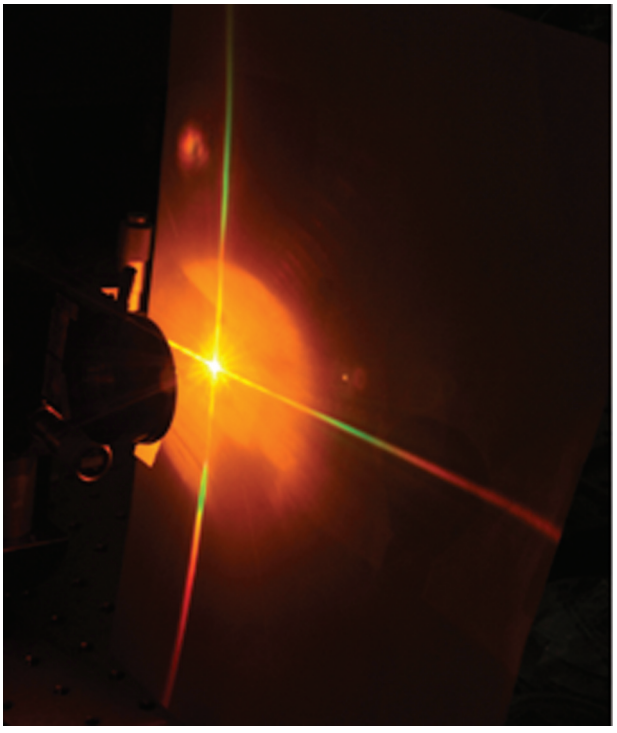

Figure 3. Characteristic cross diffraction pattern of the reflected wave due to the structure geometry.

lattice, writing **g** as a linear combination of a set of 2D primitive reciprocal lattice vectors ($\mathbf{b}_1$,$\mathbf{b}_2$), i.e. $\mathbf{g} = p\mathbf{b}_1 + q\mathbf{b}_2$, p, q integers, the cut-off condition is met for $\frac{d}{\lambda} = \frac{1}{n}\sqrt{p^2 + q^2}$ where n is the refractive index of the diffraction medium, λ is the wavelength of the incident radiation and d is the periodicity in the planes perpendicular to the propagation direction. In air ($n = 1$) four diffraction channels open, corresponding to

$(p, q) = (1, 0), (0, 1), (-1, 0), (0,-1)$, when $\frac{d}{\lambda} \geq 1 \Rightarrow d \geq \lambda$.

Therefore, as one moves to wavelengths smaller than 600 nm (or frequencies larger than 500 THz, i.e. in the visible range) diffraction patterns start to appear, the sharpness of which reflects the long-range order in the structure. In the diffraction pattern of Figure 3 one can clearly observe the cut off for the "red part" of the visible.

In order to focus the beam at the sample centre, the diffraction pattern was observed as the sample was translated along the beam axis. When the pattern colors were visible and well-separated, like the example of Figure 3, the focused beam was near the structure centre.

Figure 4 shows the normalized transmission results from our woodpile structure, and compares them with corresponding simulation data. The simulation data have been obtained using the CST Microwave studio® software. The geometrical structure parameters used in the simulations were obtained from cross-sectional SEM images of the actual structures. For the simulations shown in Figure 4a structure of three unit cells (12 layers) along propagation direction (or stacking direction) was considered, consisted of elliptical silver cylinders, intersecting with their neighbors (for the simulation of silver the Drude dispersion model has been used, with plasma frequency 1.37×10^{16} sec^{-1}, and collision frequency 8.5×10^{13} sec^{-1}). The cylinders have been considered made of bulk metal, due to the fact that the metal coating in the actual structures has thickness (~30–50 nm) significantly larger than the metal skin depth (~12 nm) in this frequency regime. (Simulations comparing bulk metal cylinders with 30 nm metal-coated dielectric cylinders in single-unit-cell thick structures gave almost identical results, confirming the accuracy of the bulk-metal approximation.) The structure parameters employed in the simulations (see Figure 4–right panel) were lattice constant d = 600 nm, unit cell height h = 848.5 nm, and the small (R_1) and the big (R_2) radii of the elliptical cylinders were R_1 = 60 nm and R_2 = 180 nm. The simulation curves have been obtained for normal incidence ($\theta = 0$) and for oblique incidence, TE polarization (incident electric field direction maintained constant), to account for the fact that in the experiment, due to the focusing of the incident beam, exact normal incidence was not possible, and moreover, to show the sensitivity of the measurement on the incidence angle.

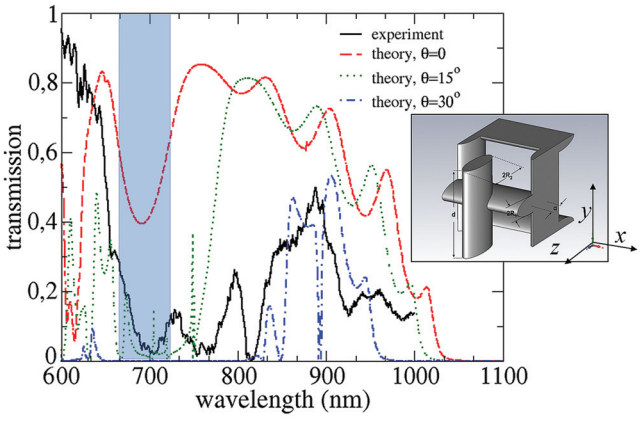

Figure 4. Experimental (black line) and theoretical transmission spectra of metalized woodpile structures with 600 nm periodicity and three unit-cell thickness. In the right panel the geometrical features of the structure unit cell are shown. The structure in the simulations has been considered as infinite in the *x*-*y* plane (using periodic boundary conditions). The simulation curves have been obtained for normal incidence ($\theta = 0$, i.e. propagation along *z*) and for oblique incidence, TE polarization (incident electric field always parallel to the *y* -axis). The shadow marks the bandgap of the structure for normal incidence.

From Figure 4a decrease in transmission between 660–720 nm can be observed (see shadowed region), both in experimental and theoretical ($\theta = 0$) data, corresponding to the red color of the optical spectrum (the transmission dip is centered at around 698 nm, i.e. ~430 THz). At shorter wavelengths (<660 nm), the disagreement between the experimental plots and the theoretical curves is mainly due to the very narrow bands and gaps appearing at those wavelengths. For example, we can observe a theoretical dip at around 610 nm with spectral width about 20 nm, and some even narrower peaks (e.g. a peak at 610 nm for $\theta = 15°$). However, it is difficult to observe so narrow peaks experimentally, due to scattering. Thus, the spectrometer shows only a broad peak which is the superposition of all these narrow bands and gaps. The disagreement between the theory and experiment in wavelengths larger than 750 nm is not only due to the non-unique propagation direction considered in the experiment, but also due to the diffraction losses at the edges of the experimental structure, due to the small structure area, comparable to that of the incident beam (in the simulations the structure in the perpendicular to the propagation directions has been considered as infinite). Such diffraction effects and losses are source of disagreement between theory and experiment also in the shorter than 660 nm wavelength region.

In order to confirm that the observed transmission dip around 700 nm was due to the existence of a periodicity-induced bandgap and not other reasons, such as the diffracted light not being collected by the spectrometer or plasmonic resonances due to metal film granularity, the simulations were repeated for a similar structure of double unit cell size and gave indeed the expected scaling of the bandgap wavelength.

While there has been a lot of active research in the modelling of three-dimensional metallic nanostructures, their realization has lacked behind, mainly due to the lack of a combination of suitable fabrication techniques and available materials. Direct laser writing is fundamentally the only technology that can provide high resolution three-dimensional nanostructures with full control over the structure details; however, it has not been fully implemented in metal nanostructure fabrication, as the materials which are most suitable for high-resolution DLW fabrication are dielectrics. With our current work we have shown that it is possible to fabricate high resolution, selectively metalized structures, opening the possibilities to a variety of applications,

from high-pass filters, to low-threshold lasers, directional antennas and three-dimensional isotropic metamaterials for imaging and microscopy applications.

A serious drawback in the applicability of such metallic structures though is the high losses, stemming from the high losses of the metal in the optical regime. Various ways are currently attempted to reduce losses, ranging from shape optimization to material (metal) optimization. A recent approach to overcome losses by using gain media, which is fully compatible with the DLW fabrication technique, seems to be a particularly promising approach, which, besides loss reduction, it can lead to the generation of active photonic media.

To conclude, we have fabricated and characterized metal-coated woodpile photonic crystals at the near IR to optical region, with 600 nm periodicity and resolution below 100 nm. Using sol-gel chemistry, direct laser writing and electroless plating metallization techniques, we were able to create the appropriate polymer network, fabricate the structures and metalize them selectively. The structures showed ohmic behavior, and a photonic gap in the visible region of the spectrum. This is the first time that 3D metallic structures with bandgap in the visible range were fabricated, opening thus the way for the design and fabrication of 3D optical components, isotropic optical metamaterials, and optical sensors.

Acknowledgements

This work was partly funded by the ITN TOPBIO (PITN-GA-2010-264362). V.P. was supported by the EU Marie Curie Fellowship Program: FASTQUAST (PITN-GA-2008-214962). K.T. by the GSRT grant I. I. Herakleitos We would like to thank Mrs. Aleka Manousaki and Ms Maria Kayambaki for expert technical assistance with SEM and conductivity measurements, respectively. We would also like to thank Prof. Petros Rakitzis for access to his laboratory. This research was supported by Dr. Athanasios Gavrielides from the AFOSR/EORD London Office via the grant FA8655-11-1-3090.

Received: December 14, 2011
Published online: January 26, 2012

[1] S. John, *Phys. Rev. Lett.* **1987**, *58*, 2486.
[2] E. Yablonovitch, *Phys. Rev. Lett.* **1987**, *58*, 2059.
[3] K. M. Ho, C. T. Chan, C. M. Soukoulis, *Phys. Rev. Lett.* **1990**, *65*, 3152.
[4] J.-M. Lourtioz, H. Benisty, V. Berger, J.-M. Gerard, D. A. Maystre, *Tchelnokov Towards Nanoscale Photonic Devices*, Springer **2008**.
[5] M. M. Sigalas, C. T. Chan, K. M. Ho, C. M. Soukoulis, *Phys. Rev. B* **1995**, *52*, 11744.
[6] D. F. Sievenpiper, M. E. Sickmiller, E. Yablonovitch, *Phys. Rev. Lett.* **1996**, *76*, 2480.
[7] A. Moroz, *Phys. Rev. Lett.* **1999**, *83*, 5274.
[8] I. El-Kady, M. M. Sigalas, R. Biswas, K. M. Ho, C. M. Soukoulis, *Phys. Rev. B.* **2000**, *62*, 15299.
[9] C. Luo, S. Johnson, J. Joannopoulos, J. Pendry, *Opt. Express* **2003**, *11*, 746.
[10] K. M. Ho, C. T. Chan, C. M. Soukoulis, R. M. Biswas, *Sol. Stat. Comm.* **1994**, *89*, 413.
[11] A. V. Akimov, A. A. Meluchev, D. A. Kurdyukov, A. V. Scherbakov, A. Holst, V. G. Golubev, *Appl. Phys. Lett.* **2007**, *90*, 3.
[12] G. von Freymann, S. John, M. Schulz-Dobrick, E. Vekris, N. Tetreault, S. Wong, V. G. Kitaev, *Appl. Phys. Lett.* **2004**, *84*, 224.
[13] X. D. Yu, Y. J. Lee, R. Furstenberg, J. O. White, P. V. Braun, *Adv. Mater.* **2007**, *19*, 1689.
[14] Y. Y. Cao, X. Z. Dong, N. Takeyasu, T. Tanaka, Z. S. Zhao, X. M. Duan, S. Kawata, *Appl. Phys.A* **2009**, *96*, 453.
[15] Y. Y. Cao, N. Takeyasu, T. Tanaka, X. M. Duan, S. Kawata, *Small* **2009**, *5*, 1144.
[16] S. Y. Lin, J. Moreno, J. G. Fleming, *Appl. Phys. Lett.* **2003**, *83*, 380.
[17] S. Y. Lin, J. G. Fleming, I. El-Kady, *Opt. Lett.* **2003**, *28*, 1909.
[18] J. G. Fleming, S. Y. Lin, I. El-Kady, R. Biswas, K. M. Ho, *Nature* **2002**, *417*, 52.
[19] H. B. Sun, S. Matsuo, H. Misawa, *Appl. Phys. Lett.* **1999**, *74*, 786.
[20] S. Kawata, H. B. Sun, T. Tanaka, K. Takada, *Nature* **2001**, *412*, 697.
[21] M. Deubel, G. Von Freymann, M. Wegener, S. Pereira, K. Busch, C. M. Soukoulis, *Nat. Mater.* **2004**, *3*, 444.
[22] C. N. LaFratta, J. T. Fourkas, T. Baldacchini, R. A. Farrer, *Angew. Chem.-Int. Edit.* **2007**, *46*, 6238.
[23] M. P. Stocker, L. J. Li, R. R. Gattass, J. T. Fourkas, *Nat. Chem.* **2011**, *3*, 223.
[24] M. Farsari, B. N. Chichkov, *Nat. Photonics* **2009**, *3*, 450.
[25] Q. Sun, S. Juodkazis, N. Murazawa, V. Mizeikis, H. Misawa, *J. Micromech. Microeng.* **2010**, *20*, 5.
[26] G. von Freymann, A. Ledermann, M. Thiel, I. Staude, S. Essig, K. Busch, M. Wegener, *Adv. Funct. Mater.* **2010**, *20*, 1038.
[27] J. Fischer, M. Wegener, *Opt. Mater. Express* **2011**, *1*, 614.
[28] C. M. Soukoulis, M. Wegener, *Nat. Photonics* **2011**, *5*, 523.
[29] J. B. Pendry, *Phys. Rev. Lett.* **2000**, *85*, 3966.
[30] J. K. Gansel, M. Thiel, M. S. Rill, M. Decker, K. Bade, V. Saile, G. von Freymann, S. Linden, M. Wegener, *Science* **2009**, *325*, 1513.
[31] M. S. Rill, C. Plet, M. Thiel, I. Staude, G. Von Freymann, S. Linden, M. Wegener, *Nat. Mater.* **2008**, *7*, 543.
[32] *Electroless Plating, Fundamentals and Applications*, (Eds: G. O. Mallory, J. B. Hajdu), American Electroplaters and Surface Finishers Society, Orlando, FL, **1990**.
[33] S. Hrapovic, Y. L. Liu, G. Enright, F. Bensebaa, J. H. T. Luong, *Langmuir* **2003**, *19*, 3958.
[34] Y.-S. Chen, A. Tal, D. B. Torrance, S. M. Kuebler, *Adv. Funct. Mater.* **2006**, *16*, 1739.
[35] A. Radke, T. Gissibl, T. Klotzbücher, P. V. Braun, H. Giessen, *Adv. Mater.* **2011**, *23*, 3018.
[36] N. Takeyasu, T. Tanaka, S. Kawata, *Appl. Phys.A* **2008**, *90*, 205.
[37] P. Nagpal, S. E. Han, A. Stein, D. Norris, *Nano Lett.* **2008**, *8*, 3238.
[38] K. Terzaki, N. Vasilantonakis, A. Gaidukeviciute, C. Reinhardt, C. Fotakis, M. Vamvakaki, M. Farsari, *Opt. Mater. Express* **2011**, *1*, 586.
[39] M. Farsari, M. Vamvakaki, B. N. Chichkov, *J. Opt.* **2010**, *12*, 124001.
[40] C. Schizas, V. Melissinaki, A. Gaidukeviciute, C. Reinhardt, C. Ohrt, V. Dedoussis, B. N. Chichkov, C. Fotakis, M. Farsari, D. Karalekas, *Int. J. Adv. Manuf. Technol.* **2010**, *48*, 435.
[41] M. Farsari, A. Ovsianikov, M. Vamvakaki, I. Sakellari, D. Gray, B. N. Chichkov, C. Fotakis, *Appl. Phys. A* **2008**, *93*, 11.
[42] B. Jia, D. Buso, Jv. Embden, J. Li, M. Gu, *Adv. Mater.* **2010**, *22*, 2463.
[43] A. Ovsianikov, X. Shizhou, M. Farsari, M. Vamvakaki, C. Fotakis, B. N. Chichkov, *Opt. Express* **2009**, *17*, 2143.
[44] A. Ovsianikov, J. Viertl, B. Chichkov, M. Oubaha, B. MacCraith, L. Sakellari, A. Giakoumaki, D. Gray, M. Vamvakaki, M. Farsari, C. Fotakis, *ACS Nano* **2008**, *2*, 2257.
[45] F. Claeyssens, E. A. Hasan, A. Gaidukeviciute, D. S. Achilleos, A. Ranella, C. Reinhardt, A. Ovsianikov, S. Xiao, C. Fotakis, M. Vamvakaki, B. N. Chichkov, M. Farsari, *Langmuir* **2009**, *25*, 3219.
[46] D. Roundy, J. Joannopoulos, *Appl. Phys. Lett.* **2003**, *82*, 3835.
[47] F. García-Santamaría, J. F. Galisteo-López, P. V. Braun, C. López, *Phys. Rev. B* **2005**, *71*, 195112.